ROBUST ENTRY NAVIGATION USING HIERARCHICAL FILTER ARCHITECTURES REGULATED WITH GATING NETWORKS

Robert H. BISHOP
Olivier DUBOIS-MATRA
The Center for Space Research
The University of Texas at Austin
Austin, TX, 78712
Email: rhbishop@mail.utexas.edu

Todd ELY
NASA Jet *Propulsion Laboratory*
California Institute of Technology
Mail Stop 301-125L
4800 Oak Grove Drive
Pasadena, CA 91109-8099
E-Mail: Todd.A.Ely@jpl.nasa.gov

ABSTRACT–*The application of a hierarchical mixture of experts architecture to martian entry navigation during the highly dynamic hypersonic pre-parachute deploy phase is investigated. The entry navigation filter design is approached in a nontraditional way by processing accelerometer and gyro data in an extended Kalman filter as if they were external measurements. A dynamics model suitable for use in an extended Kalman filter processing accelerometer measurements is developed.*

KEYWORDS–Mars entry navigation, hierarchical mixture of experts, inertial measurement unit (IMU) navigation, dead-reckoning.

INTRODUCTION

On-going investigations are aimed at developing precision navigation and orbit determination techniques capable of adaptive and autonomous operations for highly accurate navigation and event detection during interplanetary cruise, planetary approach, and in-situ planetary operations to support planetary exploration missions. The focus of recent efforts has been on the interplanetary cruise phase using an autonomous monitoring component based on a hierarchical mixture-of-experts (HME) algorithm for model identification [1]-[5]. The success of this project leads naturally to the idea that a modified HME approach might be applicable to planetary entry wherein active guidance requires accurate and robust precision navigation. Generally, during the upper atmospheric hypersonic entry phase, the only observations available are provided internally by a strapdown inertial measurement unit (IMU). Physical and dynamical constraints usually prevent access to external measurements, such as altimeters. In this paper, we examine the utility of the HME during the highly dynamic hypersonic pre-parachute deploy entry phase when only IMU data are available.

Typically a navigation system utilizing a recursive algorithm (such as an extended Kalman filter) has two main components: a state propagation component and a state update component. Both the state propagation and state update are environment and measurement model-dependent. Conventional wisdom suggests that the navigation system should utilize IMU data (when available) to *aid* the navigation system during the state

propagation phase, thereby eliminating the need for modeling the non-gravitational dynamics. All the accelerations acting on the spacecraft, modulo gravity, are assumed to be accurately measured via the IMU, and external measurements (such as altimetry) are used to update the state when available. The beauty of IMU-aided inertial navigation is that it negates the requirement for an accurate entry dynamics model. Yet, many questions remain. Can conventional IMU-aided inertial navigation be used to realize *precision landing* in the highly uncertain entry environment at Mars? Is it a robust approach able to deal effectively with IMU data gaps?

When there are no external measurements available, the IMU-aided inertial navigation process reduces to what is known as *dead-reckoning navigation.* During dead-reckoning there is no state update in the navigation system since there are no external measurements. It is possible to include stochastic models of the expected measurement errors in the IMU as part of the estimation state vector, thereby including the effects of measurement uncertainty in the filter estimation error covariance, hence improving the knowledge of the accuracy of the state estimate. Nevertheless, dead-reckoning navigation is *open-loop*, hence error growth is expected without bound.

From a navigation system perspective, the difficulty in achieving precision landing on Mars stems from the fact that in the upper atmosphere, where there is sufficient time and available lift to actively guide out any delivery and initial state knowledge errors, there are no external measurements available for navigation, hence the guidance must depend only on IMU dead-reckoning. Once the heat shield is jettisoned and the altimeter, now exposed to the external environment, provides measurements to the navigation filter (assisted by the IMU), the spacecraft is on the parachute and cannot be actively guided using lift modulation. During this phase of entry, descent, and landing (EDL), the navigation uncertainty is significantly reduced, but guidance cannot compensate for any existing state errors. In the final phase of EDL, the parachutes are jettisoned and the altimeter and LIDAR (or other hazard avoidance sensor) are available. Guidance can now actively be utilized to maneuver the vehicle, however, there is not sufficient time to make large excursions to hit a pinpoint landing. The challenge is, working within the constraints of nonavailability of sensors, to provide the most accurate navigated state and on-board computation of the uncertainty in that estimated state. In some sense, it becomes a race to reach parachute deploy conditions before the navigation state error uncertainty renders the state estimate essentially useless to guidance.

In this paper, we present a solution to the entry navigation problem that utilizes IMU data in a nontraditional way. The question that we pose is this: Is it desirable to utilize IMU measurements in a recursive filter to update the state estimate, and then employ a spacecraft entry model to propagate the state between available IMU measurements? The inclusion of other external measurements would not be prohibited, but indeed they could be readily incorporated in the filtering process whenever available. This work is done with an eye towards implementation of a HME filter bank in which the filters are parameterized with various atmospheric and other spacecraft parameters.

We begin to answer the following questions: During the pre-parachute deploy entry phase utilizing IMU data only, can the HME improve trajectory knowledge during EDL in the presence of highly uncertain atmospheric models? Can the HME improve atmosphere modeling via its inherent model identification capabilities? To address these questions, we first develop a dynamics model suitable for use in an extended Kalman filter processing IMU accelerometer measurements. The development is motivated by the desire to construct a model that can accurately represent the motion of an entry spacecraft with enough sophisti-

cation to capture the essential elements of the dynamics, yet be amenable to application to optimal recursive filtering, i.e., sufficient analytic differentiability. We confirm that under ideal conditions, the proposed model can accurately duplicate an actual entry trajectory. By ideal conditions, we mean that the initial state is precisely known, all aerodynamic coefficients and associated parameters are known, and the bank angle is known. Since we do not have access to any actual entry trajectory data, we rely instead on high-fidelity "truth" simulation results generated by NASA Langley Research Center using the POST simulator[1] and the NASA Johnson Space Center "truth" simulation results generated by the SORT simulator[2].

Notations The convention adopted here is for vectors and matrices to be **boldface** and scalars to be *italic* type. For example, the magnitude of the vector $\mathbf{r}$ is denoted by r. The vector inner (dot) product is denoted by $\odot$ and the outer (cross) product by $*$. The standard Euclidean norm of a vector is denoted by $\| \bullet \|$.

REFERENCE FRAMES

In this section, the various references frames are defined. A more thorough review of the reference frames will be required as the system design matures to determine optimum reference systems for the various subsystems.

Planet-Centered Reference Frame: The planet-centered inertial frame is depicted in Figure 1, where $\mathbf{e}_3^i$ lies along the planet spin axis, and $\mathbf{e}_1^i$ and $\mathbf{e}_2^i$ lie in the equatorial plane and form a right-handed coordinate system.

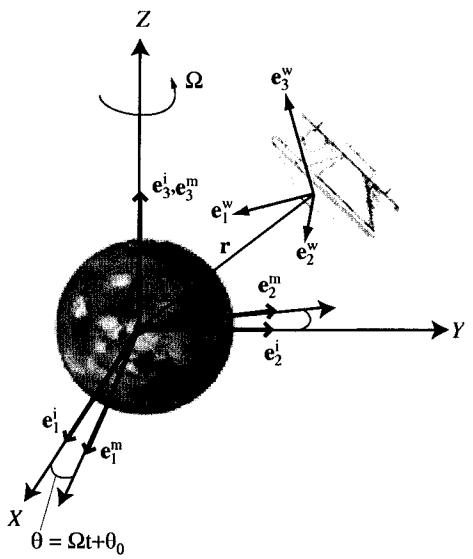

Figure 1: Planet-centered inertial and planet-centered rotating reference frames.

[1]Contact Scott Striepe at S.A.Striepe@larc.nasa.gov for information on POST

[2]Contact Tim Crain at tim.crain1@jsc.nasa.gov for information on SORT

We assume the planet is rotating at a constant rate, denoted by Ω, that is

$$\mathbf{\Omega} = \begin{bmatrix} 0 \\ 0 \\ \Omega \end{bmatrix} .$$

As illustrated in Figure 1, the planet-centered rotating frame unit vector $\mathbf{e}_3^m$ is aligned with the planet-centered inertial frame unit vector $\boldsymbol{e}_3^i$. The planet-centered rotating frame rotates relative to the planet-centered inertial frame at a constant rate, $\Omega := \|\mathbf{\Omega}\|$, through the angle $\theta = \Omega t + \theta_0$.

Wind Frame: The wind frame, defined with respect to the atmosphere, is depicted in Figure 2. The spacecraft velocity relative to the atmosphere is given by

$$\mathbf{v}_{rel} = \dot{\mathbf{r}} - \mathbf{\Omega} * \mathbf{r} ,$$

where $\mathbf{r}$ is the position of the entry vehicle in the planet-centered inertial frame. The unit vector $\mathbf{e}_1^w$ is defined as

$$\mathbf{e}_1^w = \frac{\mathbf{v}_{rel}}{v_{rel}} , \tag{1}$$

where $\mathbf{v}_{rel}$ is the velocity of the entry vehicle relative to the local atmosphere in the planet-centered inertial frame, $v_{rel} := \|\mathbf{v}_{rel}\|$, and the superscript "w" denotes the wind reference frame. Since the vectors $\mathbf{e}_2^w$ and $\mathbf{e}_3^w$ only need to span the "lift space," we can use the

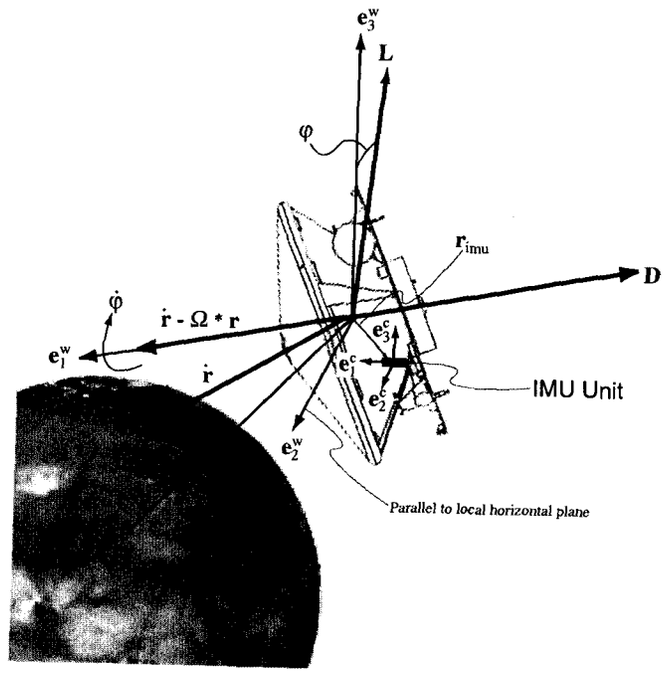

Figure 2: Wind and IMU case reference frames with lift/drag/bank angle definitions.

definitions

$$\mathbf{e}_2^w = -\frac{\mathbf{e}_1^w * \mathbf{r}}{\|\mathbf{e}_1^w * \mathbf{r}\|} \quad \text{and} \quad \mathbf{e}_3^w = \mathbf{e}_1^w * \mathbf{e}_2^w . \tag{2}$$

This means that $\mathbf{e}_2^w$ is defined with respect to the local horizontal. Also, the transformation from the wind frame to the inertial frame is given by

$$\mathbf{L}_{IW} = [\ \mathbf{e}_1^w \ \vdots \ \mathbf{e}_2^w \ \vdots \ \mathbf{e}_3^w\ ] .$$

The bank angle, denoted by φ and shown in Figure 2, is the main guidance variable. It is a rotation about the relative velocity vector, $\mathbf{e}_1^w$. When $\varphi = 0$, we have a "lift-up" condition. Similarly, when $\varphi = \pm 180°$, we have a "lift-down" condition.

IMU Case Frame: The IMU case frame is attached to the IMU unit, as depicted in Figure 2. The accelerometer package measures nongravitational accelerations in the IMU case frame, denoted by $\mathbf{a}_m^c$. Dead-reckoning navigation requires that the IMU-measured accelerations be transformed to the inertial frame for numerical integration. The transformation matrix is a function of the spacecraft attitude, which we choose to represent via the classical Euler quaternion $\mathbf{Q} \in \mathcal{R}^4$, where

$$\mathbf{Q} := \begin{bmatrix} \mathbf{q} \\ q_4 \end{bmatrix} \in \mathcal{R}^4,$$

and $\mathbf{q} = [q_1\ q_2\ q_3]^T$ subject to the constraint that $\mathbf{q}^T\mathbf{q} + q_4^2 = 1$. In terms of the quaternion components, the transformation matrix from the IMU case frame to the inertial frame is given by

$$\mathbf{T}_{IC} = \begin{bmatrix} 1-2(q_2^2+q_3^2) & 2(q_1q_2+q_3q_4) & 2(q_1q_3-q_2q_4) \\ 2(q_1q_2-q_3q_4) & 1-2(q_1^2+q_3^2) & 2(q_2q_3+q_1q_4) \\ 2(q_1q_3+q_2q_4) & 2(q_2q_3-q_1q_4) & 1-2(q_1^2+q_2^2) \end{bmatrix}. \tag{3}$$

For purposes of computing the spacecraft attitude, the IMU unit contains a gyro package that provides measurements of the relative angular velocity of the IMU case reference frame relative to the inertial reference frame, denoted by $\boldsymbol{\omega}_m$. The measured angular velocity velocity vector is integrated to obtain the attitude, represented by $\mathbf{Q}$. Nominally, the IMU unit will be installed in the spacecraft at a position offset from the spacecraft center of mass. This position is not known perfectly, and will indeed vary as the spacecraft expends fuel for attitude control purposes. A potentially significant step change in the offset of the IMU from the center of mass is expected when the heat shield separates. If the IMU offset is not properly accounted for, attitude motion will inadvertently be measured as translated acceleration. The offset of the IMU from the spacecraft center of mass is not considered here.

DEAD RECKONING NAVIGATION

The system dynamics in the inertially-fixed frame are given in the general form

$$\begin{aligned} \dot{\mathbf{r}} &= \mathbf{v} \\ \dot{\mathbf{v}} &= \mathbf{g}(\mathbf{r}) + \mathbf{T}_{IC}(\mathbf{Q})\mathbf{a}^c \\ \dot{\mathbf{Q}} &= \frac{1}{2}\mathbf{B}(\boldsymbol{\omega})\mathbf{Q} \end{aligned} \tag{4}$$

with the initial conditions

$$\mathbf{r}(t_0) = \mathbf{r}_0, \quad \mathbf{v}(t_0) = \mathbf{v}_0, \quad \mathbf{Q}(t_0) = \mathbf{Q}_0,$$

where $\mathbf{g}(\mathbf{r})$ is the acceleration due to gravity, $\mathbf{a}^c$ is the true nongravitational acceleration represented in the IMU case frame, $\mathbf{T}_{IC}$ is the transformation matrix from the IMU case

frame to the inertial frame, and $\boldsymbol{\omega} = [\omega_x\ \omega_y\ \omega_z]^T$ is the relative angular velocity vector of the IMU case frame with respect to the inertial frame. The matrix $\mathbf{B}(\boldsymbol{\omega})$ in Eq. (4) is defined to be

$$\mathbf{B}(\boldsymbol{\omega}) := \begin{bmatrix} 0 & \omega_z & -\omega_y & \omega_x \\ -\omega_z & 0 & \omega_x & \omega_y \\ \omega_y & -\omega_x & 0 & \omega_z \\ -\omega_x & -\omega_y & -\omega_z & 0 \end{bmatrix}. \tag{5}$$

Alternatively, we can represent the quaternion dynamics via

$$\dot{\mathbf{Q}} = \frac{1}{2}\mathbf{A}(\mathbf{Q})\boldsymbol{\omega} \tag{6}$$

where

$$\mathbf{A}(\mathbf{Q}) := \begin{bmatrix} q_4 & q_3 & q_2 \\ q_3 & q_4 & -q_1 \\ -q_2 & q_1 & q_4 \\ -q_1 & -q_2 & -q_3 \end{bmatrix}. \tag{7}$$

Suppose that $\mathbf{a}_m^c(t)$ and $\boldsymbol{\omega}_m(t)$ are available from the IMU. Then, dead reckoning navigation is the process of integrating over the interval $[t_0, t]$ the following equations:

$$\begin{aligned} \dot{\hat{\mathbf{r}}} &= \hat{\mathbf{v}} \\ \dot{\hat{\mathbf{v}}} &= \mathbf{g}(\hat{\mathbf{r}}) + \mathbf{T}_{IC}(\hat{\mathbf{Q}})\mathbf{a}_m^c \\ \dot{\hat{\mathbf{Q}}} &= \frac{1}{2}\mathbf{B}(\boldsymbol{\omega}_m)\hat{\mathbf{Q}} \end{aligned} \tag{8}$$

$$\tag{9}$$

where $\mathbf{g}(\hat{\mathbf{r}})$ is the modeled gravity, $\hat{\mathbf{Q}} = \left[\hat{\mathbf{q}}^T \mid \hat{q}_4\right]^T = [\hat{q}_1\ \hat{q}_2\ \hat{q}_3\ \hat{q}_4]^T$ is the estimated quaternion, $\mathbf{B}(\boldsymbol{\omega}_m)$ is the matrix defined in Eq. (5) evaluated using the measured $\boldsymbol{\omega}_m$, and $\mathbf{T}_{IC}(\hat{\mathbf{Q}})$ is the matrix in Eq. (3) evaluated using the estimated quaternion. The initial conditions are denoted by

$$\hat{\mathbf{r}}(t_0) = \hat{\mathbf{r}}_0, \quad \hat{\mathbf{v}}(t_0) = \hat{\mathbf{v}}_0, \quad \hat{\mathbf{Q}}(t_0) = \hat{\mathbf{Q}}_0,$$

and must be available *apriori* as a result of approach tracking (for $\hat{\mathbf{r}}(t_0)$ and $\hat{\mathbf{v}}(t_0)$) and from the IMU alignment (for $\hat{\mathbf{Q}}(t_0)$).

SENSOR ERROR MODELS

The accelerometers and gyros produce measurements corrupted by random errors (noise and biases), systematic biases, and other errors. The effectiveness of the navigation system (esp. dead-reckoning navigation) depends on the magnitude of the IMU errors and on the accuracy of the initial spacecraft state knowledge.

Accelerometers

The measurement of the nongravitational accelerations is corrupted by errors due to nonorthogonality and misalignment of the axes, errors due to scale factor uncertainties, random biases, and noise. The strapdown accelerometer error model can be formulated as

$$\mathbf{a}_m^c = (\mathbf{I} + \boldsymbol{\Upsilon}_a)(\mathbf{I} + \boldsymbol{\Xi}_a)(\mathbf{a}^c + \mathbf{b}_a + \boldsymbol{\epsilon}_a), \tag{10}$$

where

$$\boldsymbol{\Upsilon}_a := \begin{bmatrix} 0 & \upsilon_{a_{xz}} & -\upsilon_{a_{xy}} \\ -\upsilon_{a_{yz}} & 0 & \upsilon_{a_{yx}} \\ \upsilon_{a_{zy}} & -\upsilon_{a_{zx}} & 0 \end{bmatrix}, \quad \boldsymbol{\Xi}_a := \begin{bmatrix} \xi_{a_x} & 0 & 0 \\ 0 & \xi_{a_y} & 0 \\ 0 & 0 & \xi_{a_z} \end{bmatrix}, \quad \mathbf{b}_a := \begin{bmatrix} b_{a_x} \\ b_{a_y} \\ b_{a_z} \end{bmatrix},$$

and $(\upsilon_{a_{yz}}, \upsilon_{a_{zy}}, \upsilon_{a_{zx}}, \upsilon_{a_{xz}}, \upsilon_{a_{xy}}, \upsilon_{a_{yx}})$ are nonorthogonality and axes misalignment errors, $\mathbf{b}_a$ is the bias in the accelerometer, $(\xi_{a_x}, \xi_{a_y}, \xi_{a_z})$ are scale factor errors, and $\boldsymbol{\epsilon}_a$ is a white noise stochastic process. The nonorthogonality and axes misalignment errors, scale factor errors, and bias parameters are all modeled as zero-mean, Gaussian-distributed random constants with appropriate covariances. The noise $\boldsymbol{\epsilon}_a$ is modeled as a zero-mean, Gaussian-distributed, time-wise uncorrelated random process, with

$$E(\boldsymbol{\epsilon}_a(t)\boldsymbol{\epsilon}_a^T(\tau)) = \mathbf{V}_a(t)\delta(t-\tau),$$

where $\delta(t)$ is the Dirac delta function. If we assume that the various errors are "small," then to first-order we have

$$\mathbf{a}_m^c = (\mathbf{I} + \boldsymbol{\Upsilon}_a + \boldsymbol{\Xi}_a)(\mathbf{a}^c + \mathbf{b}_a + \boldsymbol{\epsilon}_a). \tag{11}$$

Gyros

The measurement of the angular velocity vector is corrupted by random biases, errors due to scale factor uncertainties, errors due to nonorthogonality and axes misalignments, and random noise. The gyro error model can be formulated as

$$\boldsymbol{\omega}_m = (\mathbf{I} + \mathbf{S}_g)(\mathbf{I} + \boldsymbol{\Gamma}_g)(\boldsymbol{\omega} + \mathbf{b}_g + \boldsymbol{\epsilon}_g)\ , \tag{12}$$

where

$$\mathbf{S}_g := \begin{bmatrix} S_{g_x} & 0 & \\ 0 & S_{g_y} & 0 \\ 0 & 0 & S_{g_z} \end{bmatrix}, \quad \boldsymbol{\Gamma}_g := \begin{bmatrix} 0 & \gamma_{g_{xz}} & -\gamma_{g_{xy}} \\ -\gamma_{g_{yz}} & 0 & \gamma_{g_{yx}} \\ \gamma_{g_{zy}} & -\gamma_{g_{zx}} & 0 \end{bmatrix}, \tag{13}$$

and $(\gamma_{g_{yz}}, \gamma_{g_{zy}}, \gamma_{g_{zx}}, \gamma_{g_{xz}}, \gamma_{g_{xy}}, \gamma_{g_{yx}})$ are nonorthogonality and axes misalignment errors, $\mathbf{b}_g$ is the bias in the gyro, $(S_{g_x}, S_{g_y}, S_{g_z})$ are scale factor errors, and $\boldsymbol{\epsilon}_g$ is a white noise stochastic process. The nonorthogonality and axes misalignment errors, scale factor errors, and bias parameters are all modeled as zero-mean, Gaussian-distributed random constants with appropriate covariances. The noise $\boldsymbol{\epsilon}_g$ is modeled as a zero-mean, Gaussian-distributed, time-wise uncorrelated random process, with

$$E(\boldsymbol{\epsilon}_g(t)\boldsymbol{\epsilon}_g^T(\tau)) = \mathbf{V}_g(t)\delta(t-\tau).$$

If we assume that the various errors are "small," then to first-order we have

$$\boldsymbol{\omega}_m = (\mathbf{I} + \mathbf{S}_g + \boldsymbol{\Gamma}_g)(\boldsymbol{\omega} + \mathbf{b}_g + \boldsymbol{\epsilon}_g), \tag{14}$$

The specific error parameter values depend on the choice of IMU for a particular mission. This paper describes a work-in-progress, and as such, specific key parameter values have not been selected for the analysis. In fact, the results presented herein are for IMU units providing acceleration corrupted by random noise only, that is, $\boldsymbol{\epsilon}_a$ in Eq. (11) and $\boldsymbol{\epsilon}_g$ in Eq. (14). The angular orientation of the spacecraft is assumed known perfectly. Future

work will consider the contributions of the biases and misalignments.

FILTER MODEL DEVELOPMENT

The sum of the accelerations acting on the entry vehicle is

$$\ddot{\mathbf{r}} = \mathbf{a} + \mathbf{g} \ , \tag{15}$$

where $\mathbf{a}$ are the aerodynamic accelerations ($\mathbf{a} = \mathbf{L} + \mathbf{D}$) and $\mathbf{g}$ is the gravitational acceleration. We assume that the reentry vehicle is not thrusting. Taking the time derivative of Eq. (15) yields

$$\dddot{\mathbf{r}} = \dot{\mathbf{a}} + \dot{\mathbf{g}} \ . \tag{16}$$

The time derivative of the gravity term depends on the gravity model employed. For example, if we utilize a central gravity model, then computing the time derivative yields

$$\dot{\mathbf{g}} = \left[\frac{\partial \mathbf{g}}{\partial \mathbf{r}}\right] \dot{\mathbf{r}} = -\frac{\mu}{r^3}\dot{\mathbf{r}} + 3\frac{\mu}{r^5}(\mathbf{r} \odot \dot{\mathbf{r}})\mathbf{r} \ . \tag{17}$$

Depending on the implementation of the filter, choosing the third state to be $\mathbf{a}$ rather than $\ddot{\mathbf{r}}$ eliminates the need to compute the gravity time derivative .

Referring to Figure 2, it can be seen that

$$\mathbf{a} = -D\mathbf{e}_1^w + L\left[-\mathbf{e}_2^w \sin\varphi + \mathbf{e}_3^w \cos\varphi\right] \ . \tag{18}$$

Taking the time-derivative of Eq. (18) yields

$$\dot{\mathbf{a}} = \left[\boldsymbol{\omega}^w + \dot{\varphi}\ \mathbf{e}_1^w\right] * \mathbf{a} - \dot{D}\mathbf{e}_1^w + \dot{L}\left[-\mathbf{e}_2^w \sin\varphi + \mathbf{e}_3^w \cos\varphi\right] \ , \tag{19}$$

where

$$\boldsymbol{\omega}^w = \mathbf{e}_1^w * \dot{\mathbf{e}}_1^w = \frac{\mathbf{v}_{rel} * \dot{\mathbf{v}}_{rel}}{v_{rel}^2} \ . \tag{20}$$

Substituting Eqs. (1), (2), (17), (19), and (20) into Eq. (16) yields the entry vehicle model

$$\dddot{\mathbf{r}} = \overbrace{\boldsymbol{\omega}^w * (\ddot{\mathbf{r}} - \mathbf{g}(\mathbf{r}))}^{(a)} + \overbrace{\dot{\varphi}\ \mathbf{e}_1^w * (\ddot{\mathbf{r}} - \mathbf{g}(\mathbf{r}))}^{(b)} - \dot{D}\mathbf{e}_1^w + \dot{L}\left[-\mathbf{e}_2^w \sin\varphi + \mathbf{e}_3^w \cos\varphi\right] - \left[\frac{\partial \mathbf{g}}{\partial \mathbf{r}}\right] \dot{\mathbf{r}} \ . \tag{21}$$

The entry vehicle model in Eq. (21) is interesting from several points of view. First, it is a rather straight-forward model derived from basic principles. It is amenable to computer integration, possessing singularities only when r or v_{rel} are zero; both situations are unimportant in our study. Secondly, this entry vehicle model provides direct access to the acceleration states, which should lead to improved filtering and prediction as we process the accelerometer measurements directly in the filter. Of course, the potential increase in estimation performance comes at the price of three additional states. Thirdly, and more importantly, the model provides direct insight into the various components of the vehicle motion. For example, the first term (a) represents the curvature motion in-plane, and the second-term (b) represents motion out-of-plane. The remaining terms can similarly be classified. Since we are ultimately concerned with guiding and controlling the entry vehicle motion, it is desirable to be able to quantify the in-plane and out-of-plane motion in terms of the state of the vehicle.

The dynamics in this case are simpler, but the measurement partials are significantly more complex. Additionally, the measurement partials are now model-dependent (need to know C_D, C_L and density model parameters). The question is, is it preferable to keep measurement partials model-free so that the EKF update stage is not corrupted by uncertainty in the model, but pay the price in more complex dynamics which will impact the EKF propagation stage. This question needs further investigation, but for purposes of this paper, we chose to utilize the more complex dynamics with the thought that proper "tuning" of the EKF propagation phase can account more easily for the uncertainty in the model, while keeping the EKF update stage structured so model uncertainty did not corrupt the covariance correlations. This is necessary for more precise navigation and filter stability when the first external measurement is processed by the EKF.

In the results that follow, the values of the lift coefficient, C_L, and the drag coefficient, C_D, are taken to be piece-wise constant with values taken directly from the simulation environment. This is, of course, not possible in the real-world. One area of significant work that remains is in determining an accurate and reliable model for the aerodynamic parameters that can be used in the filter. This is an on-going effort. Also, the values of the bank angle are assumed provided by an attitude determination subsystem. It may be beneficial to consider integrating the attitude determination and the trajectory navigation.

RESULTS

Three main results are presented in this section. The first is a verification of the entry dynamics model presented in the previous section. The second is a test of the robustness of the IMU active filtering process against IMU failure. The third result is a test of the hierarchical filter bank architecture in detecting the correct COSPAR atmospheric parameters in the filter.

Dynamics Model Verification

The entry dynamics described in the previous section (see Eq. (21)) were tested to verify that they can reproduce the truth trajectory under ideal conditions. The term "ideal conditions" means that the true bank angle, atmospheric density, and aerodynamic coefficients are known. A truth trajectory was generated utilizing two NASA simulations: the NASA LRC POST simulation and the NASA JSC SORT simulation for a Mars 2005-class lander ($m = 438$ kg) scenario from entry interface to parachute deployment (approximately 90 km to 10 km altitude. The results show that the total error in position at parachute deploy to be approximately *two hundred and fifty meters*, as shown in Fig. 3.

Considering the differences in the level of fidelity between the NASA simulations and the dynamics model presented here, a few hundred meters difference in the trajectory at parachute deploy is an excellent match. The differences in the trajectories are explained by the different numerical integration algorithms and stemming from the use of different gravity models (a simple J_2 model is used in the filter dynamics model whereas the NASA simulations utilize higher-order gravity models).

IMU Failure Robustness

One issue to consider is the robustness of the navigation system to gaps in the measurements. Robustness implies that the navigation system should be able to perform well in the presence of IMU measurement gaps. It is assumed here that IMU failure means that

Define the state vector to be

$$\mathbf{x} := \begin{pmatrix} \mathbf{r} \\ \mathbf{v} \\ \mathbf{a} \end{pmatrix},$$

where the components are the inertial position, $\mathbf{r}$, velocity, $\mathbf{v}$, and aerodynamic acceleration, $\mathbf{a}$. The state variable form of the dynamics can be represented as

$$\begin{aligned} \dot{\mathbf{x}}_1 &= \mathbf{x}_2 \\ \dot{\mathbf{x}}_2 &= \mathbf{g}(\mathbf{x}_1) + \mathbf{x}_3 \\ \dot{\mathbf{x}}_3 &= \mathbf{f}(\mathbf{x}, t) \end{aligned} \tag{22}$$

where

$$\mathbf{f}(\mathbf{x}, t) = (\boldsymbol{\omega}^w + \dot{\varphi}\ \mathbf{e}_1^w) * \mathbf{x}_3 - \dot{D}\mathbf{e}_1^w + \dot{L}\left[-\mathbf{e}_2^w \sin\varphi + \mathbf{e}_3^w \cos\varphi\right] .$$

With the relative velocity computed via

$$\mathbf{v}_{rel} = \mathbf{x}_2 - \boldsymbol{\Omega} * \mathbf{x}_1 ,$$

where we assume that the planet is rotating at a constant rate, denoted by Ω, we have

$$\boldsymbol{\omega}^w = \frac{(\mathbf{x}_2 - \boldsymbol{\Omega} * \mathbf{x}_1) * ([\mathbf{g}(\mathbf{x}_1) + \mathbf{x}_3] - \boldsymbol{\Omega} * \mathbf{x}_2)}{||\mathbf{x}_2 - \boldsymbol{\Omega} * \mathbf{x}_1||^2}$$

and Eqs. (1) and (2) expressed as functions of the state vector, $\mathbf{x}$, take the form

$$\mathbf{e}_1^w = \frac{\mathbf{x}_2 - \boldsymbol{\Omega} * \mathbf{x}_1}{||\mathbf{x}_2 - \boldsymbol{\Omega} * \mathbf{x}_1||}, \quad \mathbf{e}_2^w = -\frac{\mathbf{e}_1^w * \mathbf{x}_1}{\|\mathbf{e}_1^w * \mathbf{x}_1\|}, \quad \text{and} \quad \mathbf{e}_3^w = \mathbf{e}_1^w * \mathbf{e}_2^w.$$

In this paper, we assume that the atmospheric density profile in the filter can be modeled via the exponential function

$$\frac{\rho(x_1)}{\rho_o} = exp\left[-C_1 \frac{x_1 - R_M}{H_0} + C_2 \cos(\frac{2\pi(x_1 - R_M)}{H_0}) + C_3 \sin(\frac{2\pi(x_1 - R_M)}{H_0})\right] , \tag{23}$$

where $x_1 := ||\mathbf{x}_1||$, R_M is Mars equitorial radius. The atmospheric model in Eq. (23) was developed as a curve-fit to the COSPAR density model (derived from Viking lander data) [6]. Typical values for the model for a Mars 2005-class entry scenario in the lower region of the atmosphere are $\rho_0 = 3.492 \times 10^{-3}$ kg/m^3, $C_1 = 28.27$, $C_2 = 1.5607$, $C_3 = 0.3696$, and $H_0 = 300000$. In the filter bank simulations presented in this paper, these constants are varied around their nominal values to populate the filter bank.

The measurement model is given by

$$\mathbf{y} = \mathbf{T}_{CI}\mathbf{x}_3 + \boldsymbol{\epsilon}_a, \tag{24}$$

where $\mathbf{T}_{CI} := \mathbf{T}_{IC}^{-1}(\mathbf{Q})$. Recall that, for time being, we are neglecting the scale factor errors, misalignments, and biases, that is, in Eq. (11), we set $\mathbf{b}_a = \mathbf{0}$, $\boldsymbol{\Upsilon}_a = \mathbf{0}$ and $\boldsymbol{\Xi}_a = \mathbf{0}$. The measurement model in Eq. (24) is a relatively simple form for a measurement model leading to measurement partials for the EKF that are not model dependent. This nice result comes at the cost of taking the additional derivative of $\mathbf{a}$. It might also possible to consider the situation where we do not take the derivative of $\mathbf{a}$ in the dynamics, and utilize the measurement model

$$\mathbf{y} = \mathbf{T}_{CI}\left[-D\mathbf{e}_1^w + L\left[-\mathbf{e}_2^w \sin\varphi + \mathbf{e}_3^w \cos\varphi\right]\right] + \boldsymbol{\epsilon}_a . \tag{25}$$

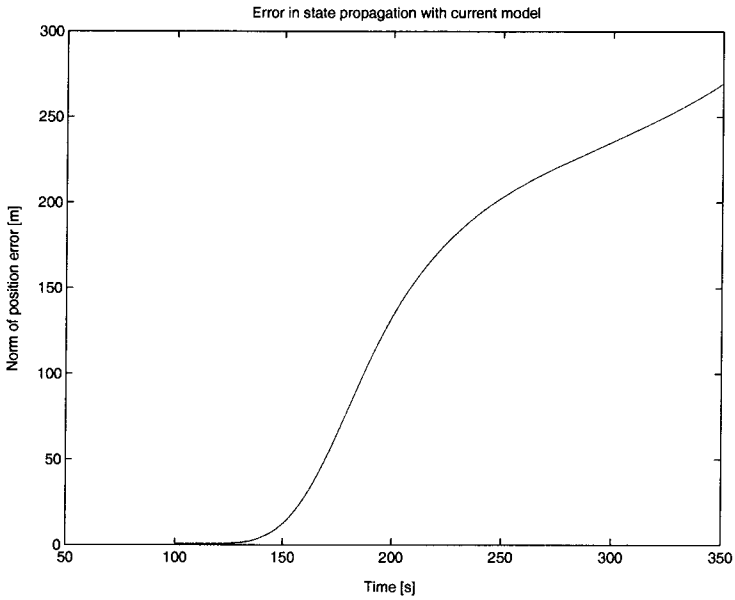

Figure 3: Position error magnitude for the entry dynamics models compared to the "truth".

both the gyroscopes and the accelerometers cease to function properly at the same time. The navigation system then has to rely on the last known acceleration and orientation of the spacecraft. This can lead to significant estimation errors, especially if the vehicle is maneuvering. The bank angle history for the scenario used in this paper is shown in Fig. 4.

In the following scenario, we assume that the IMU fails at $t = 225$ seconds and, from then on, all that is available is the last known values given by the IMU. The IMU failure occurs just before a bank maneuver (refer to Fig. 4). Three cases are considered and the resulting magnitudes of the position errors are shown in Fig. 5. First, the trajectory is propagated using dead-reckoning (shown in red) leading to a significant increase in estimation error after the IMU failure. This is an expected result. The dead-reckoning method of navigation is not robust to IMU measurement gaps. In the numerical experiment shown here, the last available IMU measurement is used in the propagation of the state until the data returns. It is understood that there may be other procedures for dealing with IMU gaps in dead-reckoning to reduce the sensitivity of the estimation process, but the fact remains that when the IMU data is missing, there does not exist a backup dynamics model to counter the error growth.

In the second numerical experiment (shown in black), the Kalman filter propagation is used to extrapolate the state forward in the absence of IMU data. Although the filter cannot account for the upcoming banking maneuvers, the flight model still allows for modeling of the aerodynamic accelerations. The result is a significantly better fit with the true trajectory for an extended period of time.

Finally, should the IMU data become available again, the dead-reckoning cannot effectively react since there is no way to reduce the state errors existing at the time of data reaquisition. On the other hand, with active Kalman filtering, the IMU data can be used to recover the state. To illustrate this, suppose that the IMU data becomes available again at $t = 250$ seconds. The resulting estimation (shown in blue in Fig. 5) shows that the filter

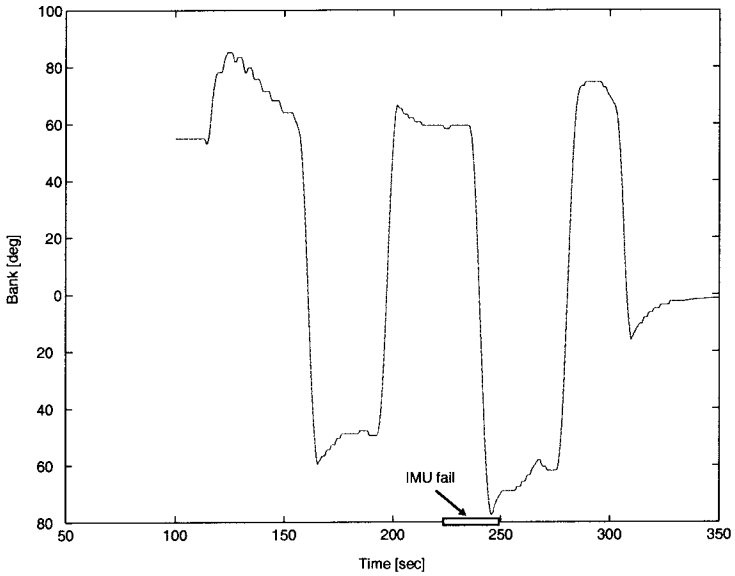

Figure 4: Bank angle history during the entry scenario used in the paper.

is able to recover the state estimate. The error and covariance plot for the acceleration corresponding to this last case is shown on Fig. 6.

Robustness also implies that the navigation system should perform well without precise knowledge of otherwise exactly known variables. The situation as it is now understood is as follows: For dead-reckoning, the robustness to the lack of knowledge of environmental parameters, such as atmospheric parameters, is high, since the process is not model dependent. Aerodynamic accelerations are measured and used directly. Only gravity models are needed, and these are relatively well-known. However, dead-reckoning is an open-loop process, hence estimation errors will always continue to grow without bound since the IMU measurements are corrupted and the initial vehicle state is not precisely known.

The issue of navigation robustness is an important issue that requires continued investigation. The early results shown in Figs. 5 and 6 strongly indicate that active filtering of the IMU data using a model-based algorithm (such as the Kalman filter) provides additional protection against IMU data gaps.

Detecting Atmospheric Parameters

The long term goal of this research is to develop a multifilter bank regulated by a gating network. Each filter would be a unique representation of a particular model of the spacecraft and/or its environment. A clear target of the filter bank would be to accurately represent the martian atmosphere. Different atmospheric density profiles, each representing a probable description of the actual conditions on Mars, can be represented in each filter, and the gating network then chooses in real time the filter the most likely to represent correctly the current density.

To illustrate how the process might work, a filter bank is constructed using three filters parameterized by the COSPAR parameters described in Eq. (23). One has an atmospheric model which is a close fit to the true density profile in the SORT simulation of the martian

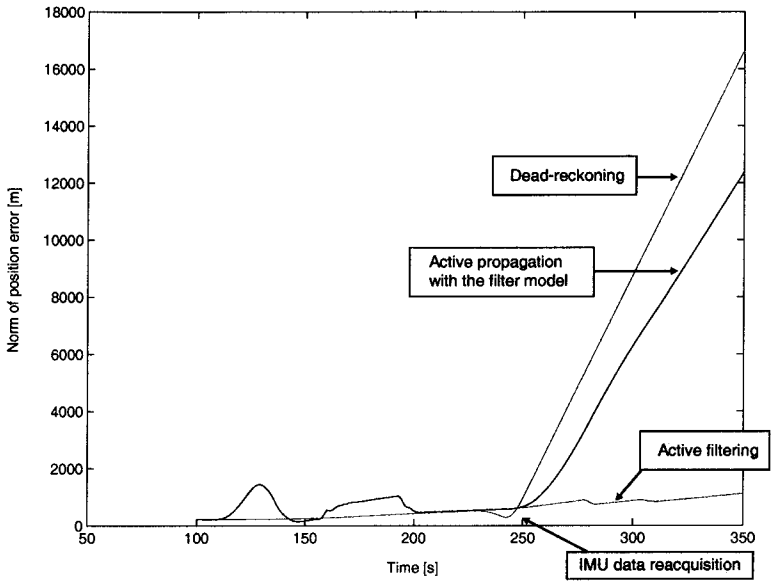

Figure 5: Comparison of position error magnitude for dead-reckoning versus active filtering.

environment for the entire entry trajectory. The SORT simulation does not utilize the COSPAR density model, but instead relies on a higher fidelity MarsGRAM density model. In the remaining two filter realizations, the coefficients of the COSPAR model in the filter are scaled by 10% during the period 250s to 300s for the second filter and by 10% during the period 300s to 350s for the third filter. The gating network assigns to each filter an activation weight as described in [2]-[3]. The activation weights are updated over time through a process which at each time involves the current probability distribution of the next measurement. The resulting activation weights are an indication of which filter is performing the best at any time.

For the current case (we assume no IMU failure), the gains are plotted in Fig. 7. Initially, the three filters are attributed the same gains. This is expected since all three filters have the same COSPAR density coefficients. At the 250s mark, the activation weight of the second filter begins to decline indicating that it's COSPAR model representation does not reflect the current environment. Since we control the simulation parameters, we know that this is indeed the situation, hence the gating network is making the correct decision. At the 300s mark, the activation weight of the third filter begins to decline indicating that it's COSPAR model representation does not reflect the current environment. Again, since we control the simulation parameters, we know that this is indeed the situation, hence the gating network is making the correct decision this time as well. In the end, the first filter ends up being selected by the network as the most likely model.

CURRENT AND FUTURE DIRECTIONS

Many issues remain to be investigated. Most importantly, it is necessary to determine the "best" approach to incorporating the "physics" associated with the entry dynamics into the hierarchical filter bank. What parameters will be well-known and which are amenable to selection via the gating network? The search for answers to this and other related questions

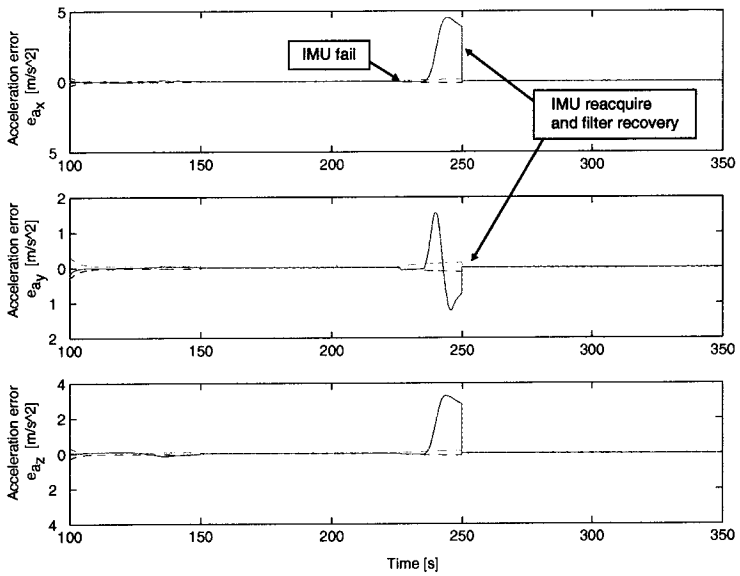

Figure 6: The error and covariance plot for the acceleration for IMU recovery.

is underway. In the remainder of this section, we present one approach.

The lift and drag acceleration magnitudes are given by

$$L = \frac{\rho(r)\dot{r}^2 C_L S}{2m} \qquad \text{and} \qquad D = \frac{\rho(r)\dot{r}^2 C_D S}{2m} \ . \tag{26}$$

Let C_L^* denote the "critical lift coefficient," that is, the lift coefficient at maximum lift-to-drag ratio. Let C_{D_o} denote the "zero-lift drag coefficient," that is, the drag coefficient when the spacecraft is not generating lift. The drag coefficient is commonly modeled by the parabolic function [7]

$$C_D = C_{D_o}\left[1 + \left(\frac{C_L}{C_L^*}\right)^2\right] \ , \tag{27}$$

where the term $(C_L/C_L^*)^2$ is the *induced drag.* At the condition of $(C_L/C_D)_{\max}$, we have $C_L = C_L^*$. Then using Eq. (27) it follows that

$$C_{D_o} = \frac{C_L^*}{2\left(\frac{C_L}{C_D}\right)_{\max}} \ , \tag{28}$$

and re-arranging yields

$$C_L = 2C_{D_o}\left(\frac{C_L}{C_D}\right)_{\max}\left(\frac{C_L}{C_L^*}\right) \ . \tag{29}$$

For convenience, we denote the ratio between the lift coefficient and the critical lift coefficient as

$$\lambda := \frac{C_L}{C_L^*} \ . \tag{30}$$

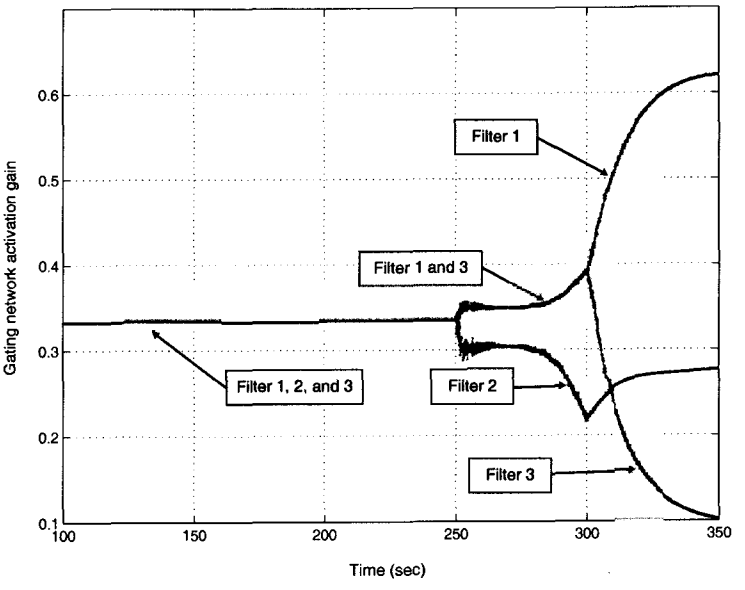

Figure 7: Activation weights for identifying the best-fit COSPAR model.

With λ thus defined, the lift and drag magnitudes can be re-written as

$$\begin{aligned} L &= \left[2\beta_m \left(\frac{C_L}{C_D}\right)_{\max}\right] \lambda q(r,\dot{r}) \\ D &= \left[\beta_m(1+\lambda^2)\right] q(r,\dot{r}) \ , \end{aligned} \tag{31}$$

where $q(r,\dot{r})$ is the dynamic pressure given by

$$q(r,\dot{r}) = \frac{1}{2}\rho(r) \left\|\dot{\mathbf{r}} - \boldsymbol{\Omega} * \mathbf{r}\right\|^2 = \frac{1}{2}\rho(r) v_{rel}^2 \ , \tag{32}$$

and the ballistic coefficent is

$$\beta_m := \frac{m}{C_{D_o} S} \ .$$

The time-derivatives of $\dot{L}$ and $\dot{D}$ are given by

$$\begin{aligned} \frac{\dot{L}}{L} &= \frac{2\dot{\mathbf{v}}_{rel} \odot \mathbf{v}_{rel}}{v_{rel}^2} - \frac{\dot{\mathbf{r}} \odot \mathbf{r}}{H_o r}\mathcal{X}(r) + 2\frac{\dot{\beta}_m}{\beta_m} + \frac{\dot{C}_L}{C_L} \\ \frac{\dot{D}}{D} &= \frac{2\dot{\mathbf{v}}_{rel} \odot \mathbf{v}_{rel}}{v_{rel}^2} - \frac{\dot{\mathbf{r}} \odot \mathbf{r}}{H_o r}\mathcal{X}(r) + \frac{\dot{\beta}_m}{\beta_m} + \frac{2\lambda^2}{1+\lambda^2}\left[\frac{\dot{C}_L}{C_L} - \frac{\dot{C}_L^*}{C_L^*}\right] \ , \end{aligned} \tag{33}$$

where

$$\mathcal{X}(r) := C_1 + 2\pi C_2 \sin\left[\frac{2\pi(r-R_M)}{H_0}\right] - 2\pi C_3 \cos\left[\frac{2\pi(r-R_M)}{H_0}\right]$$

and

$$\dot{\mathbf{v}}_{rel} = \mathbf{x}_3 - \boldsymbol{\Omega} * \mathbf{x}_2 \ ,$$

The entry vehicle motion is fully described if we also know the "control" inputs $\varphi(t)$ and $\lambda(t)$ and the parameters β_m and $(C_L/C_D)_{\max}$. The spacecraft is thus defined by two parameters,

β_m and $(C_L/C_D)_{\max}$. This model requires knowledge of aerodynamic coefficients that are not readily measured in-flight directly with the IMU accelerations. There may exist better representations for the aerodynamics. The HME filter strategy could be designed such that lift and drag model parameters are part of the decision space, along with density parameters.

Future work needs to focus on the physical modeling appropriate for the filter structure described in the previous sections. In particular, we need to better understand how the aerodynamics of a hypersonic capsule are represented, and how the inclusion of a sensor for stagnation pressure could be utilize in the filter in conjunction with the aerodynamic model.

Other areas of work on the horizon include studying the effects of IMU measurement biases and misalignments on the navigation errors, integration of attitude estimation into the filtering process, and consideration of stagnation pressure measurement.

CONCLUSIONS

The application of a hierarchical mixture of experts architecture to martian entry navigation during the highly dynamic hypersonic pre-parachute deploy phase was investigated. It was proposed to utilize an approach that includes processing accelerometer and gyro data in an extended Kalman filter as if they were external measurements. A dynamics model suitable for use in an extended Kalman filter processing accelerometer measurements was developed and demonstrated to be an accurate representation of the entry dynamics in comparison with high-fidelity NASA simulations. At this stage in the investigations, the preliminary filtering results indicate that the entry navigation problem may be tractable using IMU accelerometer observations as measurements in an HME architecture. Also, while the pros and cons of using conventional dead-reckoning navigation over the use of a more sophisticated recursive extended Kalman filter processing IMU measurements are not firmly established, it is evident that in the event of intermittent IMU failure (that is, a failure to provide measurements for an extended period), an extended Kalman filter-based navigation algorithm is more robust and can, in fact, recover from the IMU data drop-out. Numerical experiments aimed at testing the ability of the HME to detect atmospheric parameters also provide positive indicators.

ACKNOWLEDGEMENTS

The work described in this paper was carried out at The University of Texas at Austin and at the Jet Propulsion Laboratory, California Institute of Technology, under contract with the National Aeronautics and Space Administration. The work of the first and second authors was supported by CIT/JPL grant 959577.

References

[1] Burkhart, P. D., and Bishop, R. H.,"Adaptive Orbit Determination for Interplanetary Spacecraft," *AIAA Journal of Guidance, Control, and Dynamics*, Vol. 19, No. 3, 1996, pp. 693-701.

[2] Chaer, W., Bishop, R. H., and Ghosh J., "A Mixture of Experts Framework for Adaptive Kalman Filtering," *IEEE Transactions on Systems, Man, and Cybernetics*, Vol. 27, No. 3, Part B, June 1997.

[3] Chaer, W., Bishop, R. H., and Ghosh J., "Hierarchical Adaptive Kalman Filtering for Interplanetary Orbit Determination," *IEEE Transactions on Aerospace and Electronic Systems*, Vol. 34, No. 3, 1998, pp. 1-14.

[4] Ely, T. A., Bishop, R. H., and Crain, T. P., "Adaptive Interplanetary Navigation using Genetic Algorithms," *Journal of the Astronautical Sciences*, Vol. 48, No. 2 and 3, 2000.

[5] Crain, T. P., and Bishop, R. H., "Event Detection and Identification During Autonomous Interplanetary Navigation," *AIAA Journal of Guidance, Control, and Dynamics*, accepted, to appear.

[6] Peterson G., and Bishop, R. H., "Entry Trajectory Dispersions Due to Uncertainties in the Mars Atmosphere," *8th AAS/AIAA Spaceflight Mechanics Meeting*, AAS 98-147, Monterey, CA, February 1998.

[7] Regan, Frank, J., and Anandakrishnan, Satya, M., *Dynamics of Atmospheric Re-Entry*, AIAA Education Series, American Institute of Aeronautics and Astronautics, 1993.